Spherical silica particle production by combined biomimetic-Stöber synthesis using renewable sodium caseinate without petrochemical agents

Ricky Curley[a,b], Russell A. Banta[a,b], Shane Garvey[a], Justin D. Holmes[a,b]

and Eoin J. Flynn[b*]

[a]School of Chemistry & Tyndall National Institute, University College Cork, Cork, T12 YN60, [b]Ireland. AMBER Centre, Environmental Research Institute, University College Cork, Cork, T23 XE10, Ireland.

*To whom correspondence should be addressed: Tel: +353-21-490-1961; E-mail: eoin.flynn@ucc.ie

Keywords: Stöber process, biomineralisation, spherical silica, biopolymers

Abstract

Spherical silica particles are typically made via Stöber processes. However, these processes are environmentally unsustainable. Here we report a process to synthesise spherical silica particles in a more sustainable way using sodium caseinate. Initial experiments showed that sodium caseinate can replace the typical industrial structural directing agents used to produce spherical particles. Particles of 124 nm in size were produced with 200 mg L^{-1} sodium caseinate and 81 µL sodium silicate, and particles with a bimodal size distribution (258 and 1432 nm) were produced with 400 mg L^{-1} sodium caseinate and 81 µL sodium silicate. Particles with multimodal size distributions between 363 – 1588 nm and 342 – 860 nm where produced with 200 mg L^{-1} sodium caseinate and 162 µL sodium silicate and 200 mg L^{-1} sodium caseinate and 810 µL sodium silicate, respectively. Higher concentrations of sodium caseinate and low concentrations of sodium silicate promoted Ostwald ripening. Low concentrations of sodium caseinate and high concentrations of sodium silicate promoted coalescence. Subsequent optimisation of the monodispersity using a statistical design of experiments yielded size-monodisperse silica particles with a narrower size distribution between 172 and 340 nm using sodium caseinate, calcium chloride, sodium silicate, and acetate buffer. Analysis of variance (ANOVA) and regression analyses were used to determine and quantify the relationship between reagent concentrations and particle size. A regression equation was calculated, which predicts particle size based on reagent concentration. Predicted particle sizes (189.6 nm, 197.1 nm, 204.6 nm, and 212.1 nm) and experimentally determined particle sizes (200 nm, 190 nm, 184 nm, and 196 nm) showed good agreement. The possibility of producing spherical silica particles sustainably is shown.

Introduction

Spherical silica is one of the most important and widely used materials in the world, used as a simple additive in products such as toothpaste and cement (Mason et al. 2019; Zheng et al. 2020), and in more advanced applications such as drug delivery, chromatography and sensors (Walcarius 2018; Manzano and Vallet-Regí 2020; Sobańska 2020). The production methods (Stöber and modified-Stöber) combined with the industrial scale at which spherical silica is made, is inherently environmentally unsustainable. The environmental impact of its production will continue to grow as demand for the material increases. The main problems associated with the large-scale production of silica is the use of environmentally damaging and toxic precursors. Alcoholic solvents and synthetic surfactants, such as cetyltrimethylammonium bromide (CTAB), are typically used and these have been shown to have adverse effects on the environment (Nałęcz-Jawecki et al. 2003; Capello et al. 2007). Industrially, synthetic surfactants and alcohols such as ethanol are mostly produced from petrochemical feedstocks (Knepper and Berna 2003; Scully and Orlygsson 2019). In order to address these problems while meeting the demand for spherical silica, a new method of production needs to be devised.

Some biological systems can create complex and intricate silica structures with a degree of control far beyond what materials scientists have been able to achieve. However, it is possible to draw inspiration from these natural systems to produce precipitated silica in a biomimetic way. Some studies have looked at the way biomineralisation takes place in various organisms. The exemplars are the diatom species *Thalassiosira pseudonana* and *Cylindrotheca fusiformis* (Lopez et al. 2006). These can create elaborate, hierarchical silica structures far beyond what is achievable with even the most advanced materials science methods. The formation of such structures is controlled by the interaction of specific biopolymers with silicic acid derivatives (Kotzsch et al. 2017; Chen et

al. 2019; Patwardhan and Staniland 2019). These biopolymers have developed through natural evolution, resulting in a highly controlled, bottom-up, silica production process.

Limited work has been done on trying to replicate the biomineralisation process in vitro using biopolymers to synthesise spherical silica particles. However, thus far, this work has only yielded silica particles that are non-spherical, agglomerated, or both (Coradin et al. 2002, 2003; Jia et al. 2004; Gautier et al. 2008; Demadis et al. 2009). We have identified sodium caseinate (NaCas) as an ideal candidate to act as a structure-directing agent (SDA) in synthesising spherical silica particles. NaCas is a widely used as an emulsion stabiliser in food products (Ji et al. 2015; Yerramilli and Ghosh 2017; Xi et al. 2020) as it provides stabilisation against coalescence via electrostatic and steric interactions (Bonnet et al. 2005). Casein is a family of phosphoproteins of four distinct types: α_{s1}-, α_{s2}-, β-, and κ-casein. The α_s-caseins are calcium sensitive and the κ-casein is calcium insensitive (Huppertz et al. 2018). The casein micelles are stabilised by steric stabilisation, with κ-casein forming a brush on the surface of the micelles, preventing agglomeration. Caseins can associate into small clusters via their hydrophobic sections. This surfactant-like behaviour can be exploited for use as an SDA in silica synthesis. Under acidic conditions, the carboxylic acid groups of the sodium caseinate sub-micelles are neutralised, increasing the attractive forces between the proteins, resulting in larger micelle-like aggregate structures (Belyakova et al. 2003). Furthermore, addition of calcium to a solution of NaCas has been shown to stabilise the aggregate structures into micelles of ca. 100 nm (McMahon and Oommen 2013). This stabilisation effect is thought to occur via crosslinking by ionic calcium, which prevents flocculation of the micelle structures (Dickinson et al. 2001). The role of amphiphilic CTAB is to control the condensation of silica to form spherical particles via these micelles. Silica condensation occurs around these micelles to produce spherical particles (Chien

et al. 2017; Bao et al. 2017). NaCas has this same physical property and could be used in the same way. Using a biopolymer such as NaCas as the SDA along with environmentally benign reagents could make the process for producing silica more sustainable by replacing the need to use petrochemically-derived reagents such as CTAB, tetraethyl orthosilicate (TEOS), and ethanol.

The objective of the current work was to produce sustainable silica nanoparticles using NaCas, as the SDA, and water-based chemistry. A new sustainable process was created, starting from the traditional modified-Stöber process. Initially, the ability of NaCas to function as an SDA to form spherical particles was tested. Once this ability was confirmed, optimisation of the process was performed which used NaCas, sodium silicate and acetate buffer. The particle size distributions were analysed for coalescence and Ostwald ripening. Further optimisation improved the monodispersity of the particles. The optimised and sustainable process uses NaCas, calcium chloride, sodium silicate, and acetate buffer. Thus, the most environmentally hazardous reagents that are typically used to produce silica were replaced with environmentally benign and sustainable ones. The environmental impact of producing spherical silica nanoparticles is greatly reduced by using this biopolymer-based approach.

Aside from the improvement in sustainability, there are other significant benefits of using a biomimetic approach to synthesising silica particles. A key area of interest is encapsulation of molecules within the silica particles. Of particular interest is bioencapsulation of proteins, enzymes, and living cells. Use of mild synthesis conditions, such as those used here, can prevent these sensitive molecules from being degraded during the encapsulation process (Yang et al. 2017; Sabu et al. 2018; Jackson et al. 2020). Another area where mild synthesis conditions are advantageous is drug delivery. Targeted drug delivery using silica as the delivery vehicle is an important area of research, but many drugs are highly sensitive the harsh synthesis conditions that

are typically used. A biomimetic synthesis approach using mild conditions can prevent the degradation, and in some cases improve the efficiency, of these drugs (Sheikhpour et al. 2017; Rasheed et al. 2019; Yang et al. 2020). Biomimetic silica syntheses have clear advantages over the traditional syntheses. The method reported here contributes to the field of biomimetic silica by developing a sustainable process for synthesising monodisperse silica under mild conditions, which could be beneficial for such advanced applications.

Experimental

Materials

Sodium silicate (10.6 % Na_2O, 26.5 % SiO_2) from Sigma Aldrich was used as the silicic acid source. Ammonium hydroxide (assay: 28-30 % NH_3 basis), sodium caseinate (NaCas), sodium acetate, and acetic acid were all purchased from Sigma Aldrich. Acetate buffer solution (0.05 mol L^{-1}, pH 5.94) was prepared in distilled water.

Silica preparation using ammonium hydroxide

Initial experiments used a traditional modified-Stöber synthesis which was adapted for use with NaCas (Keane et al. 2010). The experimental conditions, denoted by NC, are shown in **Table 1**. In a 100 mL flask, NaCas was added to distilled water under stirring and temperature was set to 50 °C. After dissolution of NaCas, ammonium hydroxide was added. Finally, sodium silicate was added and the resulting solution was left to react overnight in a closed vessel. The reaction mixture was then centrifuged at 14,000 rpm in an Eppendorf MiniSpin Plus microcentrifuge and the solids were washed with water, ethanol, and acetone to remove any residual reactants. The sample was then dried in an oven and characterised by SEM.

Table 1 Experimental conditions of syntheses using NaCas, sodium silicate, and ammonium hydroxide. Experiments are denoted by NC

	H_2O (mL)	Sodium Silicate (mL)	NH_4OH (mL)	NaCas (mg)	T (°C)
NC1	25	3.2	12	0.32	50
NC2	25	6.4	12	0.32	50
NC3	25	6.4	6	0.64	50
NC4	50	6.4	6	0.64	50

Silica preparation using buffer

After initial testing, it was found that high volumes of sodium silicate were not needed, with microlitres being sufficient to form the particles. This is of added benefit as less reagent is required. The experimental conditions, denoted by BF, are shown in **Table 2**. The required amount of NaCas stock solution (100 g L^{-1} NaCas in 0.05M acetate buffer, pH 5.94) was added to 50 mL of acetate buffer (0.05 mol L^{-1}, pH 5.94). Sodium silicate was subsequently added and the reaction solution was stirred in a closed vessel overnight at room temperature. The reaction solution was then centrifuged at 14,000 rpm in an Eppendorf MiniSpin Plus microcentrifuge and the solids were washed with water, ethanol, and acetone. The sample was then dried in an oven and characterised by SEM.

Table 2 Experimental conditions of syntheses using NaCas and sodium silicate. Experiments repeated under identical conditions with distilled water instead of acetate buffer are shown. All experiments repeated in triplicate. Experiments are denoted by BF

	Acetate Buffer [0.05 mol L^{-1}, pH 5.94] (mL)	Sodium Silicate (µL)	NaCas (mg L^{-1})
BF1	50	81	200
BF2	50	81	400
BF3	50	162	200
BF4	50	810	200

Silica preparation using buffer and $CaCl_2$

An experimental design (**Table 3**) was created using Minitab statistical software. A full factorial (2^3) design was used with all terms free from aliasing. The design was replicated twice in two blocks with one centre point per block. The input factors (NaCas, sodium silicate, $CaCl_2$) had two levels and their effect on the response variable (particle size) was analysed using ANOVA. Regression analysis was used to obtain a regression equation which could predict values of the response variable based on the input factors. Experimentally, the required amount of NaCas stock solution (20 g L^{-1} NaCas in 0.05M acetate buffer, pH 5.94) was added to 50 mL acetate buffer (0.05 mol L^{-1}, pH 5.94). Aliquots of 100 mmol L^{-1} $CaCl_2$ were added to this solution to give the required concentration of $CaCl_2$ as shown in **Table 3**. Finally, sodium silicate was added and the reaction was stirred in a closed vessel overnight. This procedure was also used for experiments conducted at pH 4.94, denoted by BC (**Table 4**). The reaction solution was then centrifuged at 14,000 rpm in an Eppendorf MiniSpin Plus microcentrifuge and the solids were washed with water, ethanol, and acetone. The sample was then dried in an oven and characterised by dynamic light scattering.

Table 3 Experimental conditions for 2^3 full factorial design with 2 replicates, 2 blocks, and 1 centre per block. Factors: sodium silicate, NaCas; sodium caseinate, $CaCl_2$. Response variable: PS; particle size. Each factor has two levels and each centre point is midway between these levels. All terms are free from aliasing. Block generators are the replicates

Run Order	Centre Point	Blocks	Sodium Silicate (μL)	NaCas (mg)	$CaCl_2$ (mmol L^{-1})
1	1	1	486	60	6
2	1	1	486	20	12
3	1	1	729	20	6
4	1	1	486	20	6
5	1	1	486	60	12
6	1	1	729	20	12
7	1	1	729	60	12
8	1	1	729	60	6
9	0	1	607	40	9
10	1	2	486	60	6
11	1	2	486	20	6
12	1	2	729	60	12
13	0	2	607	40	9
14	1	2	729	20	12
15	1	2	486	60	12
16	1	2	729	60	6
17	1	2	486	20	12
18	1	2	729	20	6

Table 4 Experimental conditions of syntheses using NaCas, sodium silicate and calcium chloride at pH 4.94. Experiments are denoted by BC

	Acetate Buffer [0.05 mol L^{-1}, pH 4.94] (mL)	Sodium Silicate (μL)	NaCas (mg)	$CaCl_2$ (mmol L^{-1})
BC1	50	729	40	8
BC2	50	729	80	8
BC3	50	729	120	8
BC4	50	729	160	8

Characterisation

Scanning Electron Microscopy (SEM) was used to obtain images of the silica particles. The SEM analyses were carried out on an FEI Inspect and Quanta 650, operated at either 10 or 15 kV. Each sample was adhered to a stainless-steel stub (stage) via double-sided carbon tape.

Elemental characterisation was acquired using energy-dispersive x-ray spectroscopy (EDX) on the FEI Quanta 650 instrument using Oxford Instruments INCA software.

Particle diameters were determined using ImageJ image analysis software and statistical analyses were done in OriginLab OriginPro 9.0 software.

Dynamic light scattering (DLS) measurements were conducted on a Micelle size was measured by dynamic light scattering (DLS) performed on a Malvern Panalytical Zetasizer Nano ZSP using non-invasive backscattering (NIBS) technology. The scattering angle was set at 173° and the measurement temperature was set to 20 °C. Samples were dispersed in ethanol and sonicated to give a stable solution prior to analysis. Mean size and polydispersity index (PDI) were determined using Cumulants analysis.

X-Ray Photoelectron Spectroscopy (XPS) spectra were acquired on an Oxford Applied Research Escabase XPS 230 System equipped with a CLASS VM 100 mm mean radius hemispherical electron energy analyser with multichannel detectors in an analysis chamber with a base pressure of 5.0×10^{-9} mbar. A pass energy of 50 eV, a step size of 0.7 eV and a dwell of 0.3 s was used for survey spectra which were swept twice. All core level scans were acquired with a step size of 0.1 eV, a dwell time of 0.1 s and a pass energy of 20 eV averaged over 10 scans. A non-monochromated Al-Kα X-ray source (1486.58 eV) at 100 W power (10 mA, 10 kV) was used for all scans. All spectra were acquired at a take-off angle of 90° with respect to the analyser axis and

were charge corrected with respect to the C 1s photoelectric line at 284.8 eV. Synthetic peaks are Gaussian in shape. The relative sensitivity factors used are from a CasaXPS library containing Scofield cross-sections.

Nitrogen sorption measurements were performed on a Micromeritics TriStar II surface area analyser (Micromeritics, Norcross, GA, USA). Samples were pre-treated by heating at 200 °C under nitrogen for 12 hours. The surface area was measured using the Brunauer-Emmett-Teller (BET) method. The pore volume and pore diameter data was calculated using the Barrett, Joyner and Halenda (BJH) method. Specific surface areas were calculated from the measured relative pressure in the range of P/P_0= 0.01 to P/P_0= 0.3.

Results and Discussion

Silica prepared with ammonium hydroxide

The ultimate goal is to make the synthesis of spherical silica more sustainable. We replaced CTAB with NaCas to investigate whether NaCas could function as an SDA. In order to use NaCas, ethanol could not be used as it can cause denaturation of the protein (Trejo and Harte 2010), so water was used as the solvent. Without ethanol, TEOS could also no longer be used because it is water-insoluble. Instead we chose water-soluble sodium silicate, which has the added benefit of being akin to the usual form of soluble silica found in nature (Coradin et al. 2003; van Dokkum et al. 2004). A catalyst was still required. The use of NaCas as an SDA necessitated the change of multiple components in the original synthesis. Thus, ammonium hydroxide was retained as the catalyst to minimise the number of changes made to the original system as much as possible . This new system was assessed , with a view to further modifying it to create a totally sustainable process if successful.

We produced spherical particles using NaCas, sodium silicate, water and ammonium hydroxide (**Fig. 1)**. The particles are spherical, but exhibit polydispersity. NC1 and NC3 show agglomeration, while NC2 shows some agglomeration and NC4 shows discrete particles. The particle diameters range between 283-1349 nm. These initial results were promising, as it showed that our modified system could indeed produce spherical particles. Control experiments conducted with sodium silicate, water, and ammonium hydroxide showed that no spherical particles were formed (**Fig. S1**). This is expected as there is no morphological control agent present in the system to control the morphology of the particles. The fact that spherical particles are only formed when NaCas is present suggests that NaCas acts as an effective SDA.

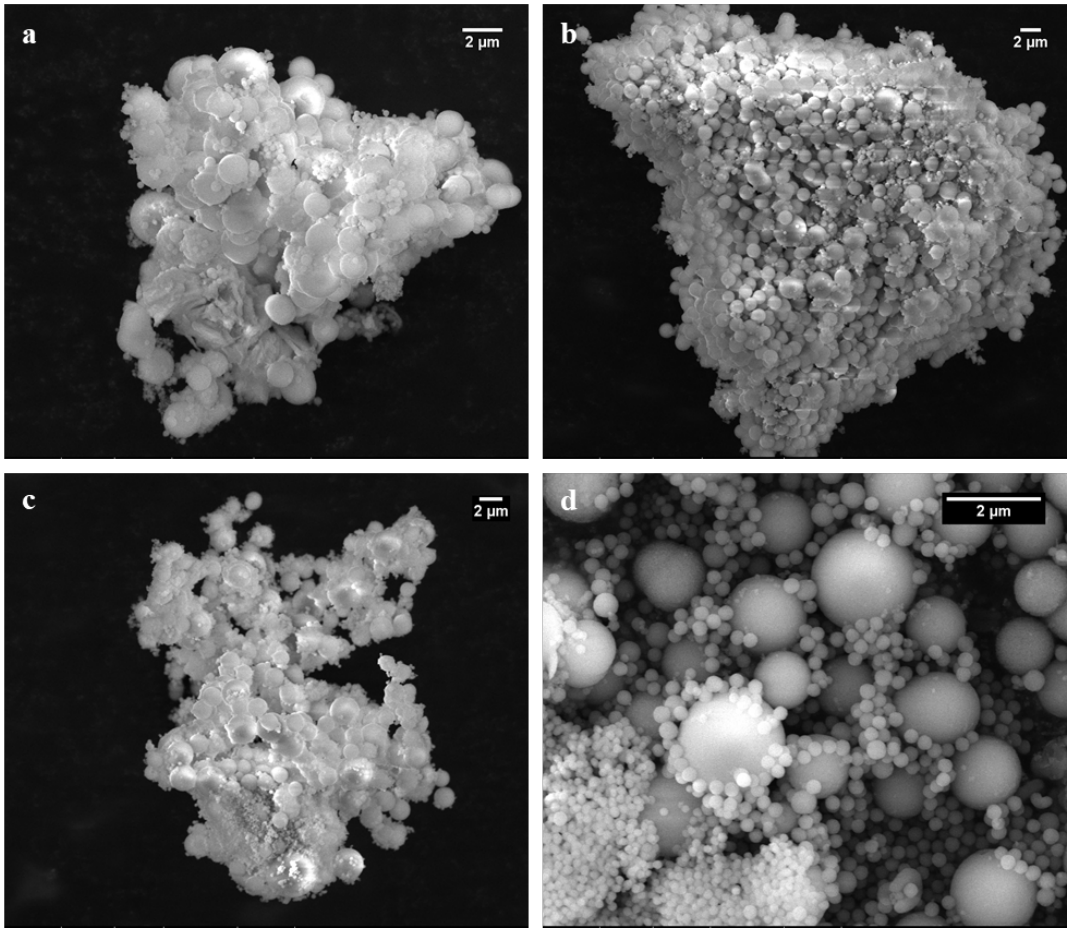

Fig. 1 SEM micrographs (a) NC1 and (b) NC2, (c) NC3, and (d) NC4. T = 50°C

These sets of experiments show that our modified system can produce spherical silica particles. Ammonium hydroxide was needed here as the catalyst to initiate the hydrolysis of sodium silicate. Two conclusions were drawn from these experiments: (1) in the absence of a morphological control agent, no spherical particles are formed in our system, and (2) in the presence of NaCas, spherical particles are formed in our system. Knowing that NaCas functions as an effective SDA in our system, we proceeded to further modify our system to increase its sustainability. Our next set of experiments used an acid catalyst in the form of acetate buffer to replace ammonium hydroxide and the role NaCas plays is investigated in detail in this new sustainable system.

Silica prepared with acetate buffer

Based on the results of our previous experiments, our next set of experiments focused on maximising the sustainability of our process. As before, sodium silicate and NaCas were used as the silica source and SDA, respectively. There was still a need to catalyse the hydrolysis of sodium silicate. Simply removing ammonium hydroxide from the system would retard silica formation. Thus, in place of ammonium hydroxide we used acetate buffer because sodium silicate hydrolyses readily in acidic media (Sierra and Guth 1999). This three component system has now eliminated the most toxic and unsustainable reagents of the modified-Stöber process; namely ethanol, ammonium hydroxide, CTAB, and TEOS. Our system uses sodium silicate as the silica source, NaCas as the SDA, and acetate buffered water, which has twofold benefit of being an environmentally benign solvent, while also promoting the hydrolysis of sodium silicate.

Our initial experiments showed that NaCas can act as an effective SDA to produce spherical particles. This was followed by experiments conducted in acetate buffer without the remaining environmentally problematic compound in the modified-Stöber process – ammonium hydroxide.

To investigate the precise role that NaCas plays in our sustainable system, dynamic light scattering (DLS) measurements of NaCas in acetate buffer were obtained. **Fig. 2** shows DLS data of NaCas in acetate buffer (0.05 mol L^{-1}, pH 5.94). The data show that at all concentrations tested, NaCas forms micelles, however in some cases they are multimodal, and showing polydispersity. Furthermore, large aggregate peaks ca. 3000nm are seen at 200, 400, and 600 mg L^{-1} NaCas and free proteins are also seen at all concentrations (< 100 nm). This polydispersity could translate into the final particles and is a likely explanation of the polydispersity seen when using the ammonium hydroxide system. Knowing that NaCas forms micelle structures in acetate buffer, we attempted to synthesise spherical silica particles using NaCas, sodium silicate, and acetate buffer.

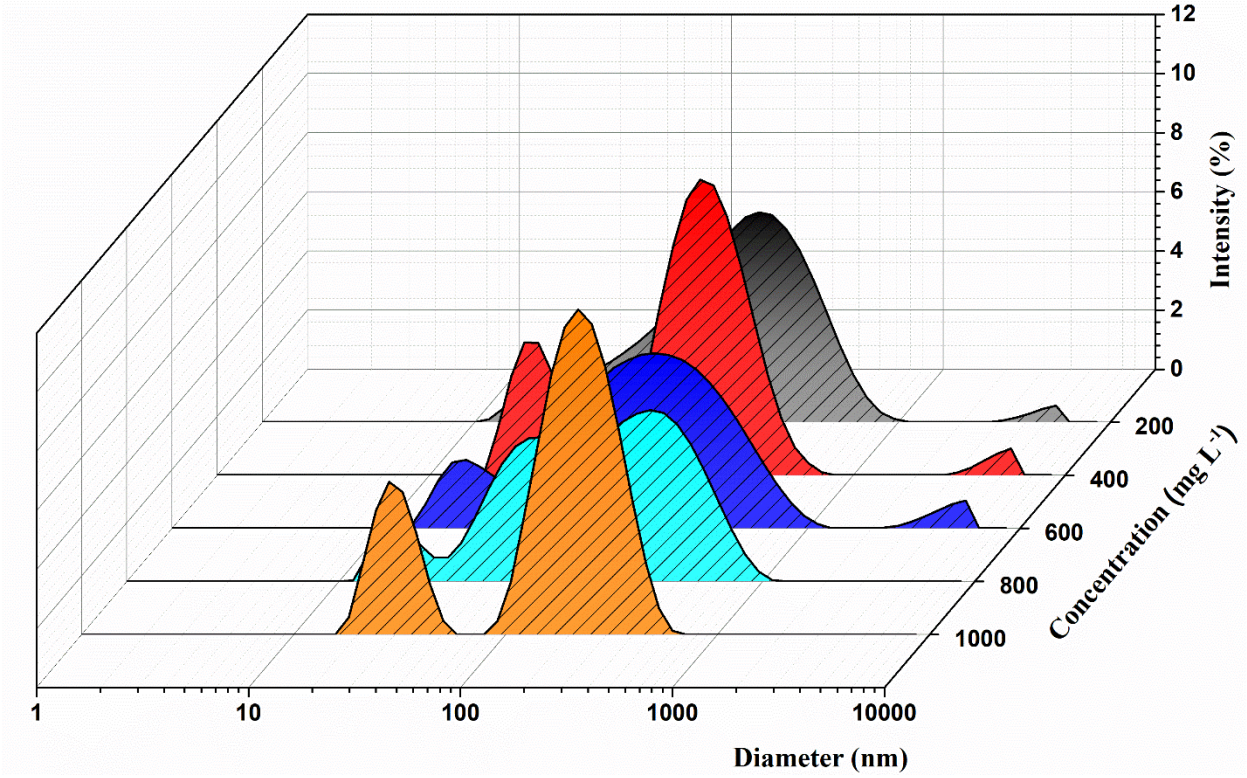

Fig. 2 DLS measurements of sodium caseinate in acetate buffer (0.05 mol L^{-1}, pH 5.94) at various concentrations

Fig. 3 shows SEM images of the spherical particles obtained with this new system. Interestingly, when these experiments were replicated using distilled water as the reaction medium, as opposed to acetate buffer, no spherical particles are formed. Instead, monoliths with no defined structure are formed (**Fig. S2**). This suggests the acidic pH promotes the conformational changes required of NaCas to form micelles. The SEM images show that the samples exhibit different degrees of polydispersity, which can be explained by the polydispersity of NaCas micelles in the DLS data of NaCas in acetate buffer.

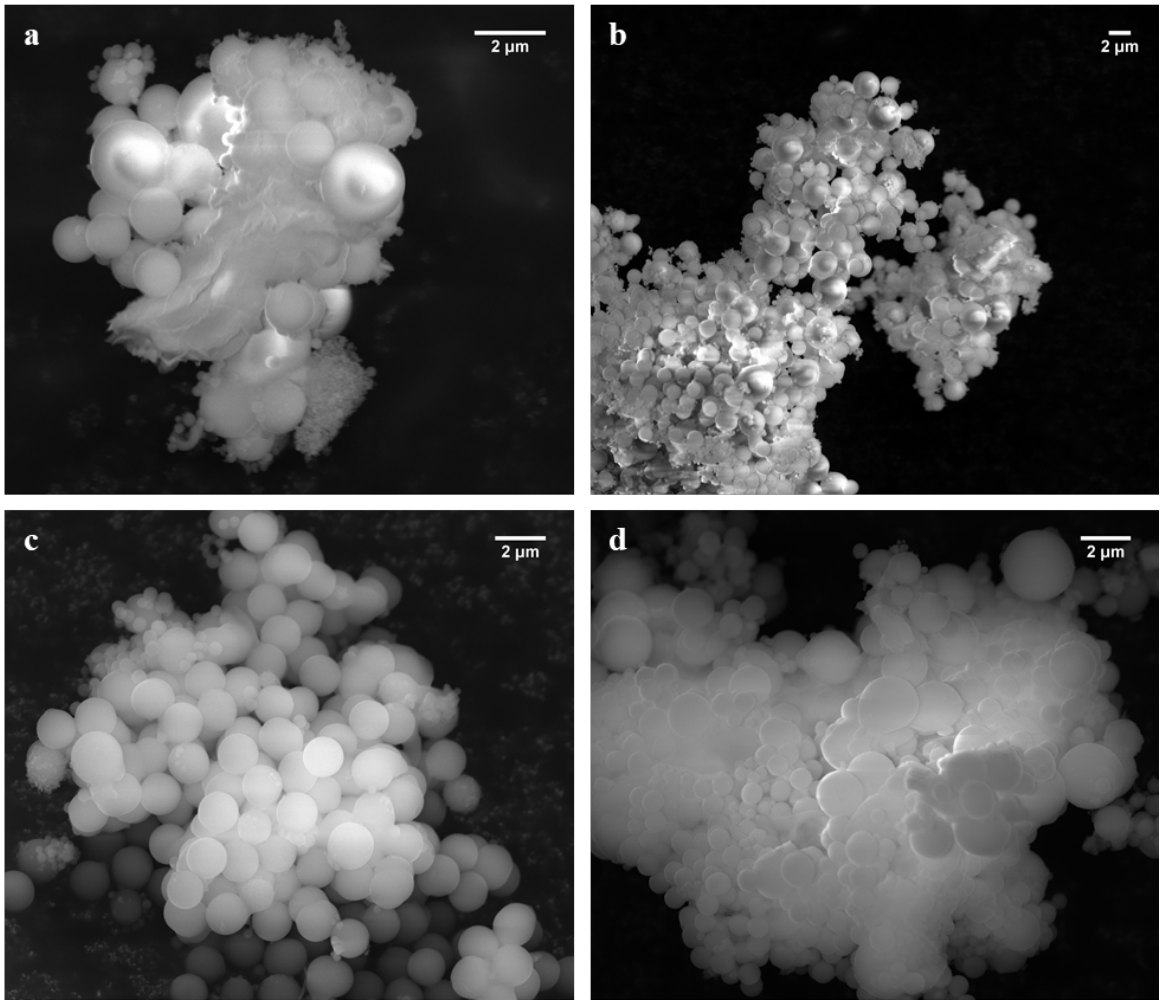

Fig. 3 SEM micrographs of silica prepared with (a) 200 mg L^{-1} NaCas (BF1), and (b) 400 mg L^{-1} NaCas (BF2), (c) 162 µL sodium silicate (BF3), and (d) 810 µL sodium silicate (BF4). Scale bars = 5 µm

Fig. 4 shows the PSDs of samples BF1 to BF4. **Fig. 4a** shows a log-normal distribution ($R^2 = 0.97$) with a mean particle diameter of 124 nm. **Fig. 4b** shows 2 peaks fitted with a combination of log-normal and Gaussian functions ($R^2 = 0.92$). At 200 mg L^{-1} NaCas, the growth of the particles is through coalescence (log-normal). At 400 mg L^{-1} NaCas, the log-normal peak centre shifts from 124 nm to 258 nm and the emergence of a Gaussian peak is seen at 1423 nm.

Coalescence occurs when particles, often of different sizes, merge to form a single particle. Accordingly, a PSD resulting from this process has a right-skewed tail, characterised by a log-normal function. Ostwald ripening occurs via material transfer from smaller, less thermodynamically stable, particles to larger particles. Larger particles, being more thermodynamically stable, grow at the expense of smaller particles. Lifshitz and Slyozov (1961), and Wagner (1961), provided mathematical descriptions of the Ostwald ripening process. This LSW model describes the PSD of particles grown via Ostwald ripening as having a left-skewed tail, with a sharp cut-off at 1.5 times the mean particle diameter. This cut-off is a consequence of the assumption in the LSW model that the solution is infinitely dilute, meaning no particle interaction takes place. In real systems, this mathematical restraint does not reflect reality, so the LSW model must be adjusted to take particle interaction into accounted. In which case, a Gaussian function provides a better description

Coalescence and Ostwald ripening can be differentiated by the shape of the distribution. Log-normal for coalescence, and Gaussian for Ostwald ripening. However, both processes are not mutually exclusive – they can, and do, coexist and overlap. Therefore, we have fitted the PSDs with a mixture of Gaussian and log-normal functions. The degree to which either process dominates depends on the experimental conditions used. Generally, Ostwald ripening results in particles which are more monodisperse than those produced via coalescence. This is because of

the log-normal distribution associated with coalescence. Therefore, analysing the PSDs can allow for optimisation of the polydispersity by understanding the experimental conditions which give rise to an Ostwald ripening-dominated mechanism.

This emergence of a Gaussian peak at higher concentrations of NaCas suggests the growth process shifts from primarily coalescence to a mixture of coalescence and Ostwald ripening, with larger particles produced. **Fig. 4c** shows a multimodal distribution fitted with Gaussian functions (R^2 = 0.98) with mean peak diameters of 363, 571, and 1588 nm. **Fig. 4d** shows a multimodal distribution fitted with a combination of Gaussian and log-normal functions (R^2 = 0.97) with mean peak diameters of 342, 698, and 860 nm. Thus, at low concentrations of sodium silicate (162 μL) growth occurs via an Ostwald ripening mechanism and at higher concentrations of sodium silicate (810 μL), a mixture of coalescence and Ostwald ripening occurs. From these experiments, in order to promote Ostwald ripening and produce more monodisperse particles, high concentrations of NaCas and low concentrations of sodium silicate are required.

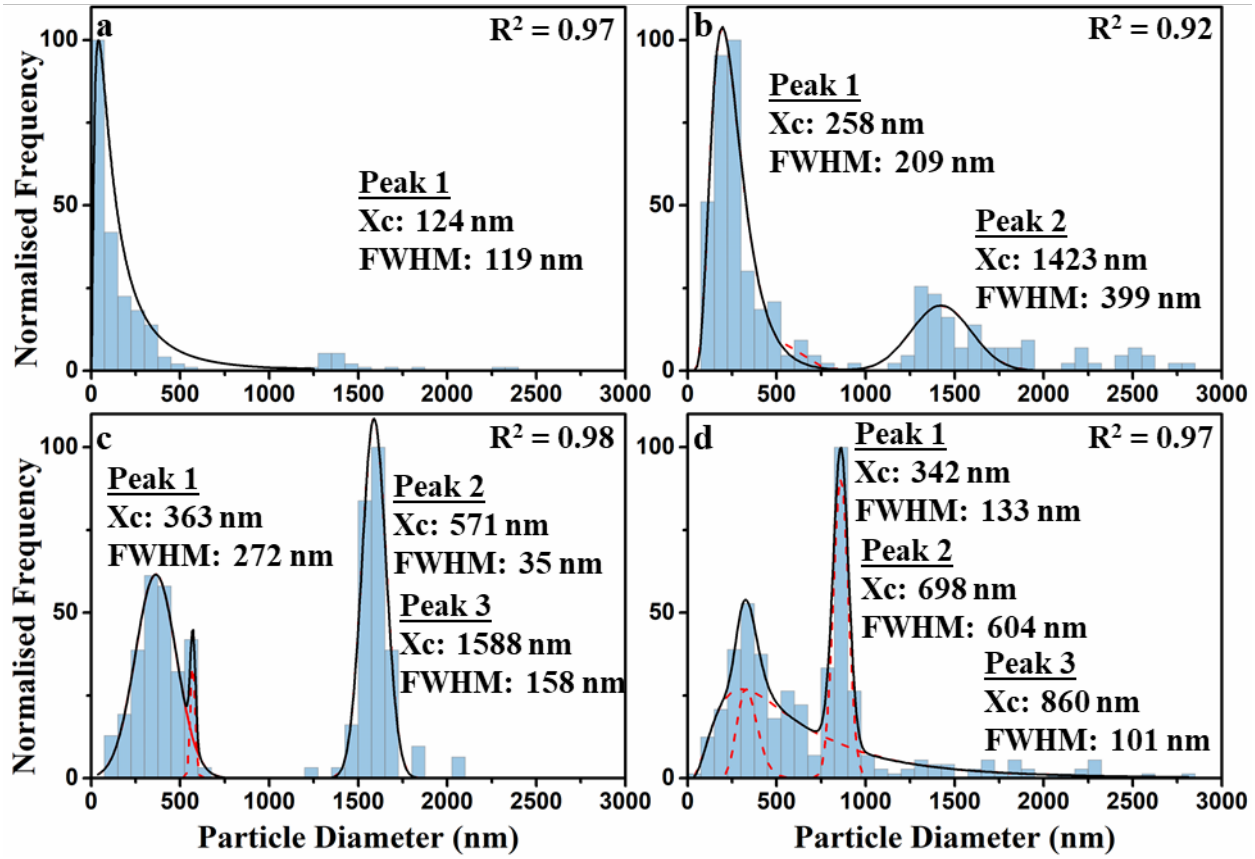

Fig. 4 PSDs of particles prepared with (a) 200 mg L^{-1} NaCas (BF1), and (b) 400 mg L^{-1} NaCas (BF2), (c) 162 µL sodium silicate (BF3), and (d) 810 µL sodium silicate (BF4)

Silica prepared with acetate buffer and calcium chloride

Our third set of experiments focused on optimising our new sustainable process for producing more monodisperse spherical silica particles. Most applications require relatively monodisperse silica. We added calcium chloride to our reaction system to stabilise the NaCas micelle. Calcium chloride has been shown to reform casein micelles from NaCas (Huppertz et al. 2018). **Fig. 5** shows distribution data from DLS measurements of NaCas with 8 mmol L^{-1} $CaCl_2$ added. The data show a marked reduction in micelle size and polydispersity compared to the NaCas system with no added $CaCl_2$ shown in **Fig. 2**. Addition of $CaCl_2$ stabilises the NaCas micelles at all

concentrations of NaCas tested. Whether or not this increase in monodispersity would translate into silica was next investigated.

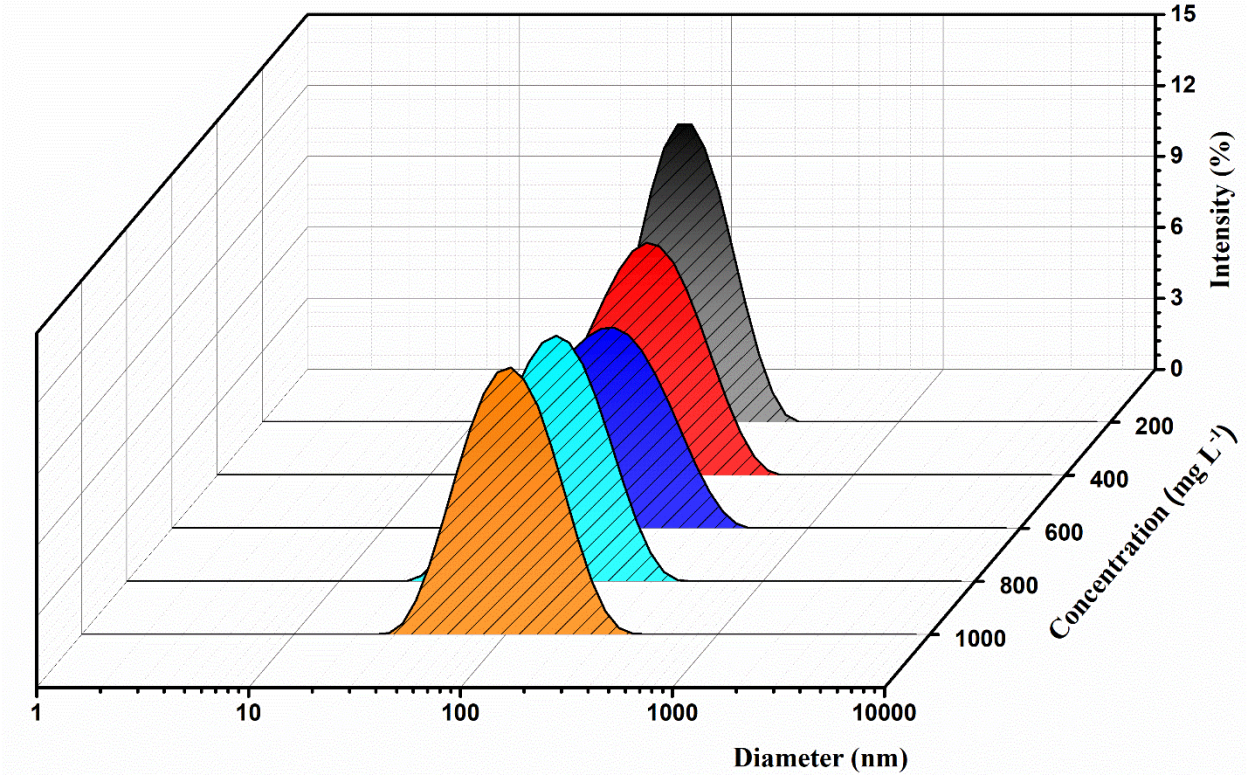

Fig. 5 Distribution data from DLS measurements of sodium caseinate at various concentrations with 8 mmol L^{-1} $CaCl_2$ in acetate buffer (0.05 mol L^{-1}, pH 5.94)

In order to optimise the synthesis and understand the influence that NaCas, sodium silicate, and $CaCl_2$ had on particle size, a statistical design of experiments (DOE) was produced to direct our methodologies. **Table S1** shows the full factorial (2^3) design used for the DOE. The design was free from aliasing, with all primary and higher order interactions analysed. The full factorial design was replicated twice in two blocks with one centre point per block. **Fig. S3** shows the normal probability plot for the residuals. **Fig. 6** shows the Pareto chart with a significance level of α = 0.05. The pareto chart indicates that four variables are statistically significant; sodium silicate,

NaCas, $CaCl_2$, and the two-way interaction between NaCas and $CaCl_2$. ANOVA (**Table S2**) also confirms these effects are statistically significant at $\alpha = 0.05$.

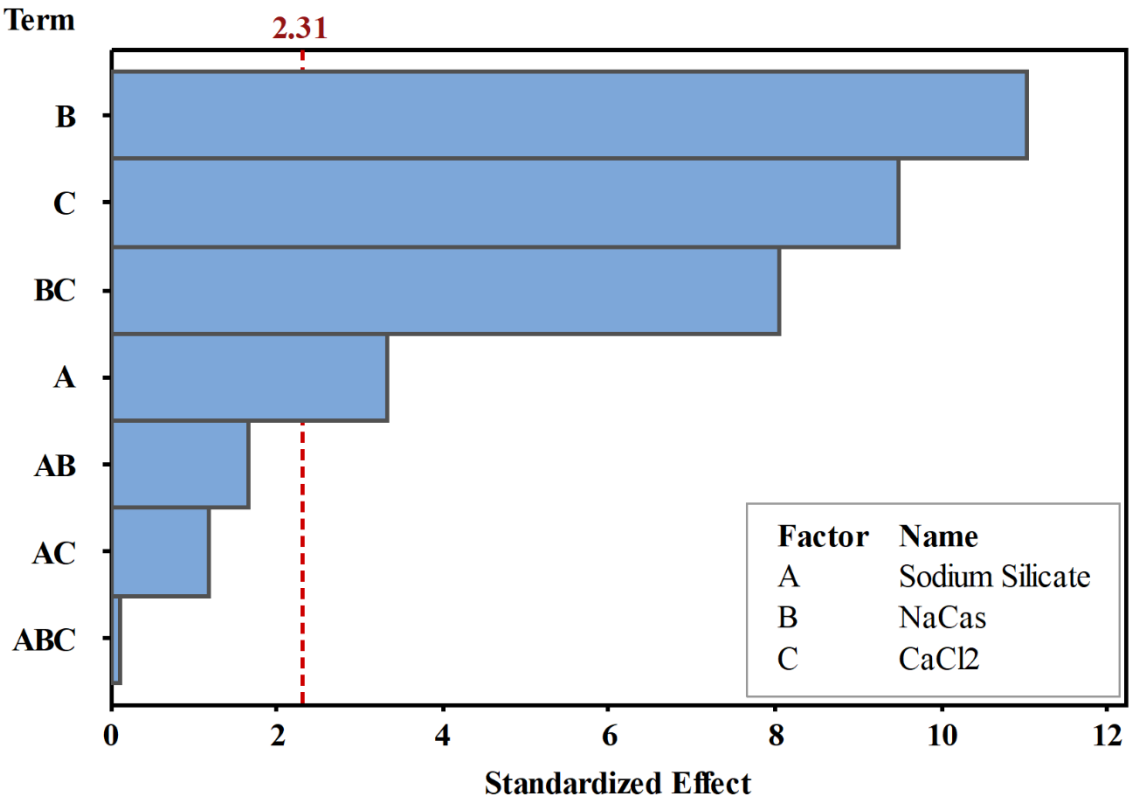

Fig. 6 Pareto chart of standardised effects (response is particle size, $\alpha = 0.05$). Significant effects are those that extend beyond the reference line (2.31)

Fig. 7 shows the main effects and interaction plots for particle size. The main effects plot (**Fig. 7a)** shows the difference in mean response (particle size) between the two levels of the factors sodium silicate, NaCas, and $CaCl_2$. The main effects plot shows that the particles produced with 486 µL sodium silicate were smaller than those produced with 728 µL. Particles produced with 20 mg NaCas were smaller than those produced with 80 mg and particles produced with 6 mmol L^{-1} $CaCl_2$ were larger than those produced with 12 mmol L^{-1} $CaCl_2$. However, because the two-way interaction of NaCas and $CaCl_2$ was statistically significant, this needs to be accounted for. The

interaction plot (**Fig. 7b**) shows when 20 mg NaCas and 12 mmol L^{-1} $CaCl_2$ were used, the smallest particles were produced, while the largest particles were produced when 60 mg NaCas and 6 mmol L^{-1} $CaCl_2$ were used. However, because the slope of the line when using 6 mmol L^{-1} $CaCl_2$ is steeper, the interaction between NaCas and $CaCl_2$ has a greater effect on particle size when 6 mmol L^{-1} $CaCl_2$ is used. The statistically significant effect that the interaction between NaCas and $CaCl_2$ has on particle size is not surprising. $CaCl_2$ is needed to conformationally change and stabilise the casein micelles in the system, which is seen in the DLS data. Furthermore, while the interaction plot shows that increasing concentration of NaCas increases particle size, the effect is not as large when using 12 mmol L^{-1} $CaCl_2$. This suggests that above a certain concentration of $CaCl_2$, the NaCas micelles are sufficiently stabilised such that addition of more $CaCl_2$ has little effect. This is confirmed in the DLS data (**Fig. 5**) which shows that the diameter of the micelles does not change significantly when NaCas concentration is increased.

Influences on the size polydispersity of the particles is also an important to understand. The polydispersity index (PDI) is a dimensionless parameter that indicates how monodisperse the sample is. The lower the PDI, the more monodisperse the sample. Values of PDI ≤ 0.1 are defined as being highly monodisperse (Bhattacharjee 2016), while values of ≤ 0.3 are considered monodisperse and acceptable for applications such as drug delivery (Mohammadpour et al. 2012; Danaei et al. 2018). **Fig. S4** shows the polydispersity index (PDI) of the particles synthesised via the DOE protocol. All of the samples have a PDI < 0.24 with the majority of the samples < 0.18, indicating good monodispersity. The lowest PDI was 0.104, corresponding to a mean particle size of 215.7 nm, indicating a high degree of monodispersity.

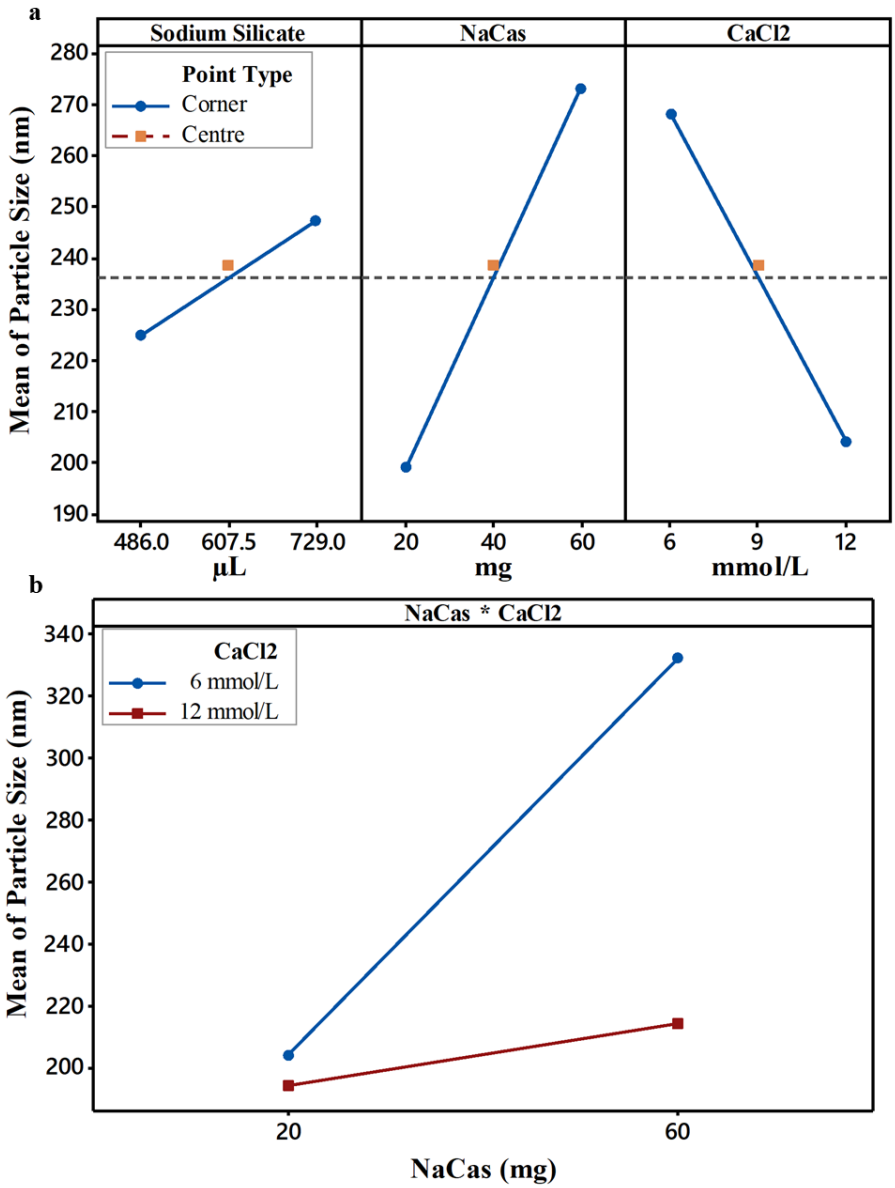

Fig. 7 (a) Main effects plots of sodium silicate, sodium caseinate, and calcium chloride and their effect on particle size. Differences between level means are shown for each factor level and are connected by a line. Orange squares are the mean response for the centre point runs. A non-horizontal line indicates a main effect is present. Dashed horizontal line shows the mean particle size for all runs (b) Interaction plot for particle size (fitted means). Non-parallel lines indicate that an interaction effect is occurring. The relationship between particle size and sodium caseinate depends on the concentration of calcium chloride

The factorial analysis of the primary and higher-order effects on particle size enables values of particle size to be predicted using regression. The regression equation obtained after stepwise regression is:

$$\text{Particle Size} = 39.5 + 0.0922\ \text{Sodium Silicate} + 5.914\ \text{NaCas} + 7.39\ CaCl_2 - 0.4509\ \text{NaCas} * CaCl_2 \quad (1)$$

Eqn. 1 shows that sodium silicate concentration has a minor effect on particle size, which is confirmed in the main effect plot, **Fig. 7a**. NaCas and $CaCl_2$ both individually and through their interaction, have a larger effect than sodium silicate on particle size. However, practical and physical limitations are presumed to exist for this relationship. As discussed earlier, the interaction effect between NaCas and $CaCl_2$ has a smaller effect on particle size at higher $CaCl_2$ concentrations. Furthermore, DLS data (**Fig. 5**) indicate that the casein micelle size does not change upon increasing NaCas concentration. However, increasing NaCas concentration increases the number of casein micelles in solution. If the rate of hydrolysis of sodium silicate is slower than the rate of nucleation, this would mean that larger particles would be formed. Furthermore, if electrostatic repulsion between forming particles is minimal and/or smaller particles are thermodynamically unstable, then particle growth could proceed by either coalescence or, Ostwald ripening, or both. Increased NaCas concentration could also lower the electrostatic repulsion between particles by stabilising the negative charge on their surfaces. The increased number of casein micelles could also reduce the interfacial energy allowing particles to grow. However, further work is needed to understand the growth dynamics of this system as other synergistic effects might also be occurring.

Table 5 shows a comparison between the predicted values of particle size and the experimental values. **Eqn. 1** was used to predict the particle size based on the input parameters sodium silicate,

NaCas, and $CaCl_2$. **Fig. 8** shows the SEM images of particles obtained from runs R1 to R4 and **Fig. 9** shows their corresponding PSDs. The experimental values for particle size of R1 and R2 show excellent agreement with the predicted values and are within the 95 % CI. The experimental values of R3 and R4 are outside the 95 % CI of the predicted value, however they still show good agreement. **Table S3** shows that the R^2 (adjusted) and the R^2 (predicted) is 93.63 and 90.39 %, respectively, meaning that there is still some variation that is unaccounted for by the regression analysis. However, based on the experimental results in **Table 5**, the regression equation performs reasonably well in predicting the particle size based on the input factors.

Table 5 Comparison of predicted and experimental values of particle size based on equation 1. Samples prepared as outlined in experimental section

Run	Sodium Silicate (µL)	NaCas[a] (mg)	$CaCl_2$ (mmol L^{-1})	Predicted PS[b] (nm)	Experimental PS (nm)
R1	486	20	8	189.6 [95 % CI (176, 202.3)]	200
R2	567	20	8	197.1 [95 % CI (185.6, 208.6)]	190
R3	648	20	8	204.6 [95 % CI (193.1, 216.1)]	184
R4	729	20	8	212.1 [95 % CI (198.4, 225.7)]	196

[a] NaCas, sodium caseinate
[b] PS, particle size; CI, confidence interval

The ability to predict particle size based on input reagent concentrations is useful as the tuneable synthesis allows for particles with a range of sizes to be synthesised. To the best of our knowledge, this is the first time that such a statistical analysis was applied to a biomimetic silica synthesis. One major problem with biomimetic syntheses to date has been the difference in quality between them and the particles produced via traditional means. The statistical analysis here is a step forward in achieving parity between biomimetically- and traditionally-synthesised silica.

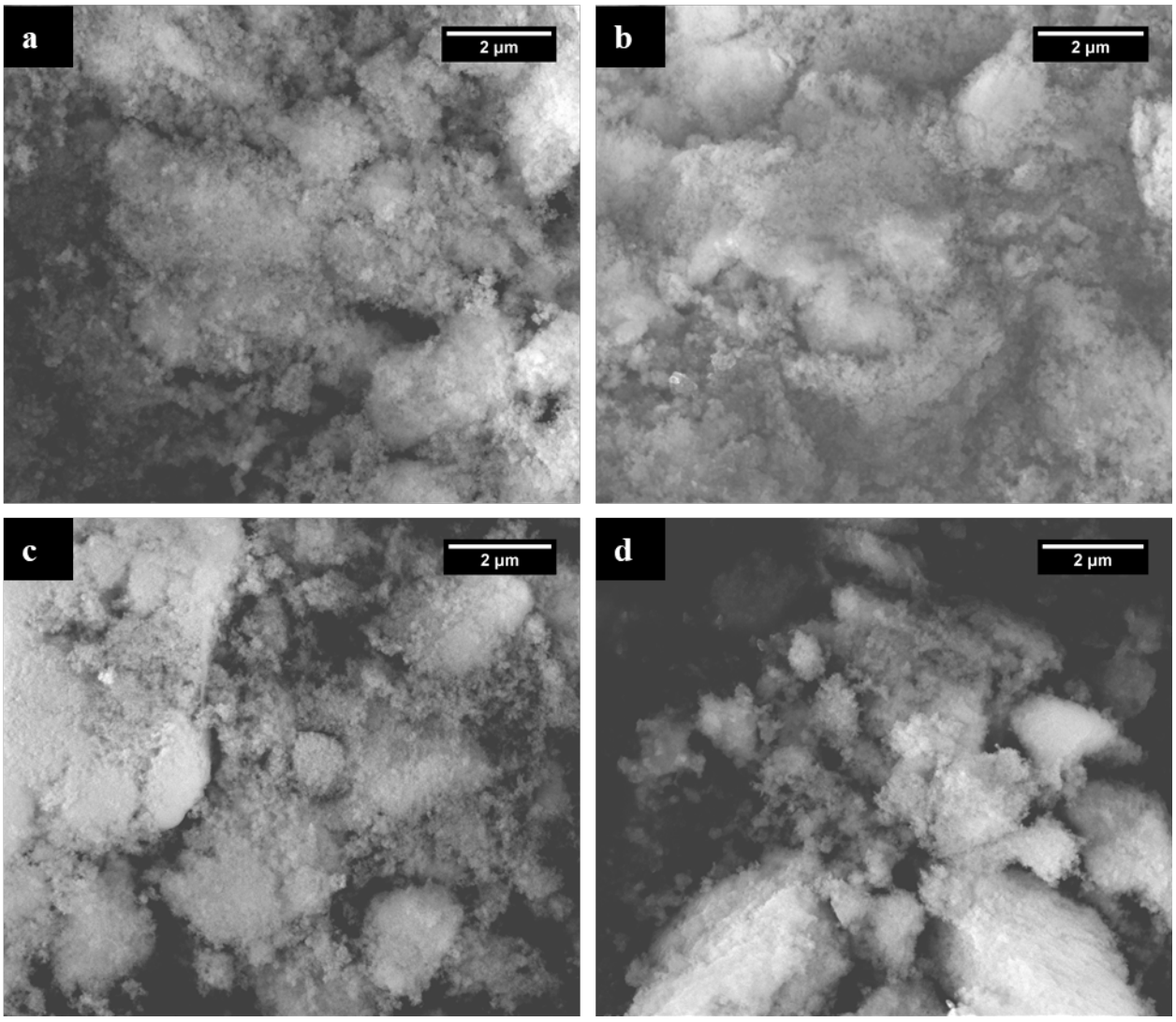

Fig. 8 SEM images of silica particles prepared with (a) 486 µL sodium silicate (R1), (b) 567 µL sodium silicate (R2), (c) 648 µL sodium silicate (R3), and (d) 729 µL sodium silicate (R4). All reactions used 20 mg NaCas and 8 mmol L^{-1} $CaCl_2$, in 50 mL acetate buffer (0.05 mol L^{-1}, pH 5.94)

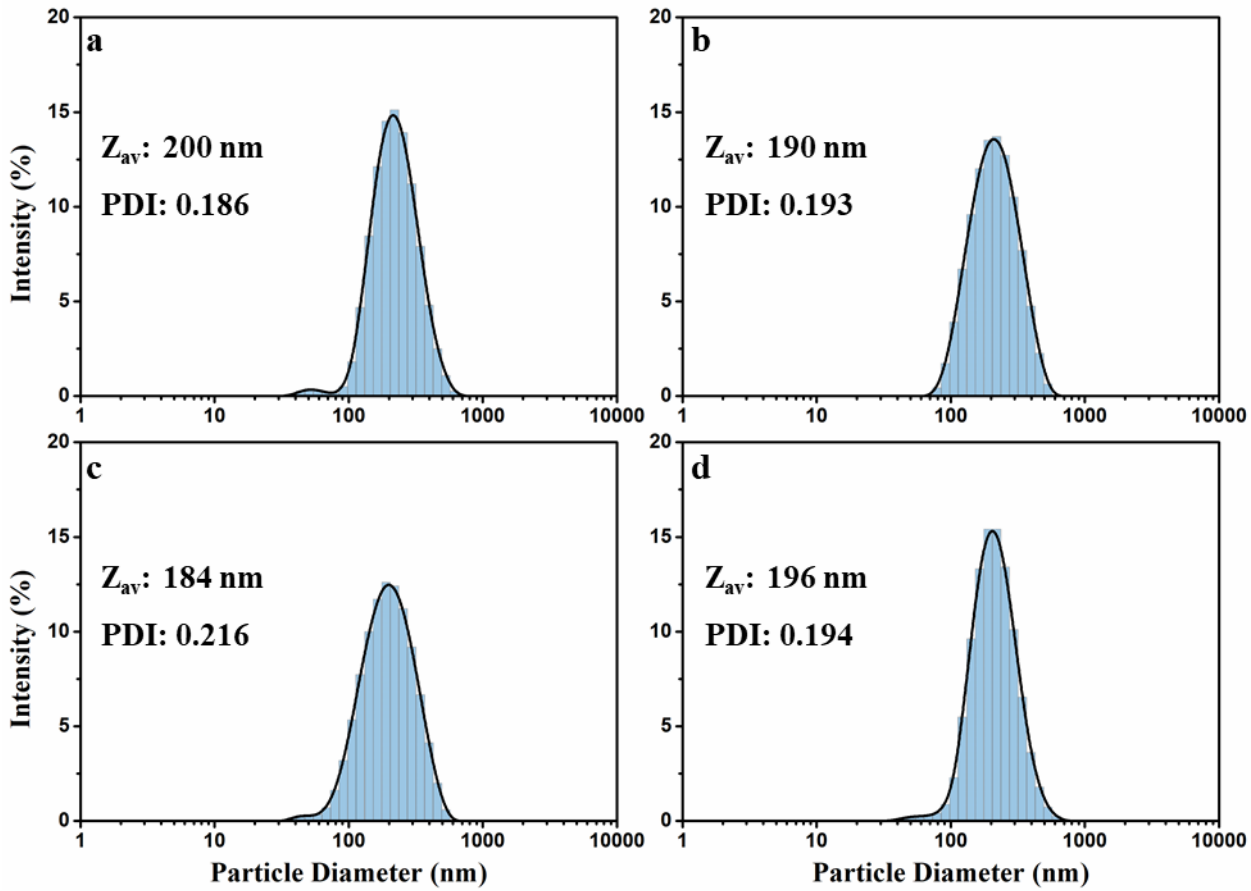

Fig. 9 PSDs from DLS measurements of silica particles prepared with (a) 486 µL sodium silicate (R1), (b) 567 µL sodium silicate (R2), (c) 648 µL sodium silicate (R3), and (d) 729 µL sodium silicate (R4). All reactions used 20 mg NaCas and 8 mmol L^{-1} $CaCl_2$, in 50 mL acetate buffer (0.05 mol L^{-1}, pH 5.94)

XPS analysis was performed to confirm the presence of silica for the R1 particles (486 µL sodium silicate, 20 mg NaCas, and 8 mmol L^{-1} $CaCl_2$). **Fig. 10** shows the O 1s and Si 2p XPS spectra, and EDX spectrum for R1. **Fig. 10a** shows the O 1s spectrum with peaks at 532.6 eV and 530.6 eV, corresponding to oxygen atoms of siloxane groups (Si-O-Si) and non-stoichiometric oxides (Si-O_x-Si), respectively (Lamastra et al. 2017). **Fig. 10b** shows the Si 2p spectrum with two peaks corresponding to Si-O-Si (103.05 eV) and Si-O-H (102.1 eV), which are indicative of SiO_2 (Li et al. 2018; Post et al. 2018). Overall, the data confirm that SiO_2 is formed. **Fig. S5** shows the nitrogen sorption isotherm and the pore size distribution of the R1 particles. The isotherm is a Type H3

hysteresis loop, which can indicate the presence of slit-shaped pores (Thommes 2010). However, there is no limiting adsorption at high P/P_0 values so interpretation of the data is hindered (Sing and Williams 2004). Thus, the values for surface area, pore volume, and pore width are given for reference only. Further work on the porosity implications of using NaCas as an SDA is needed to identify its role here.

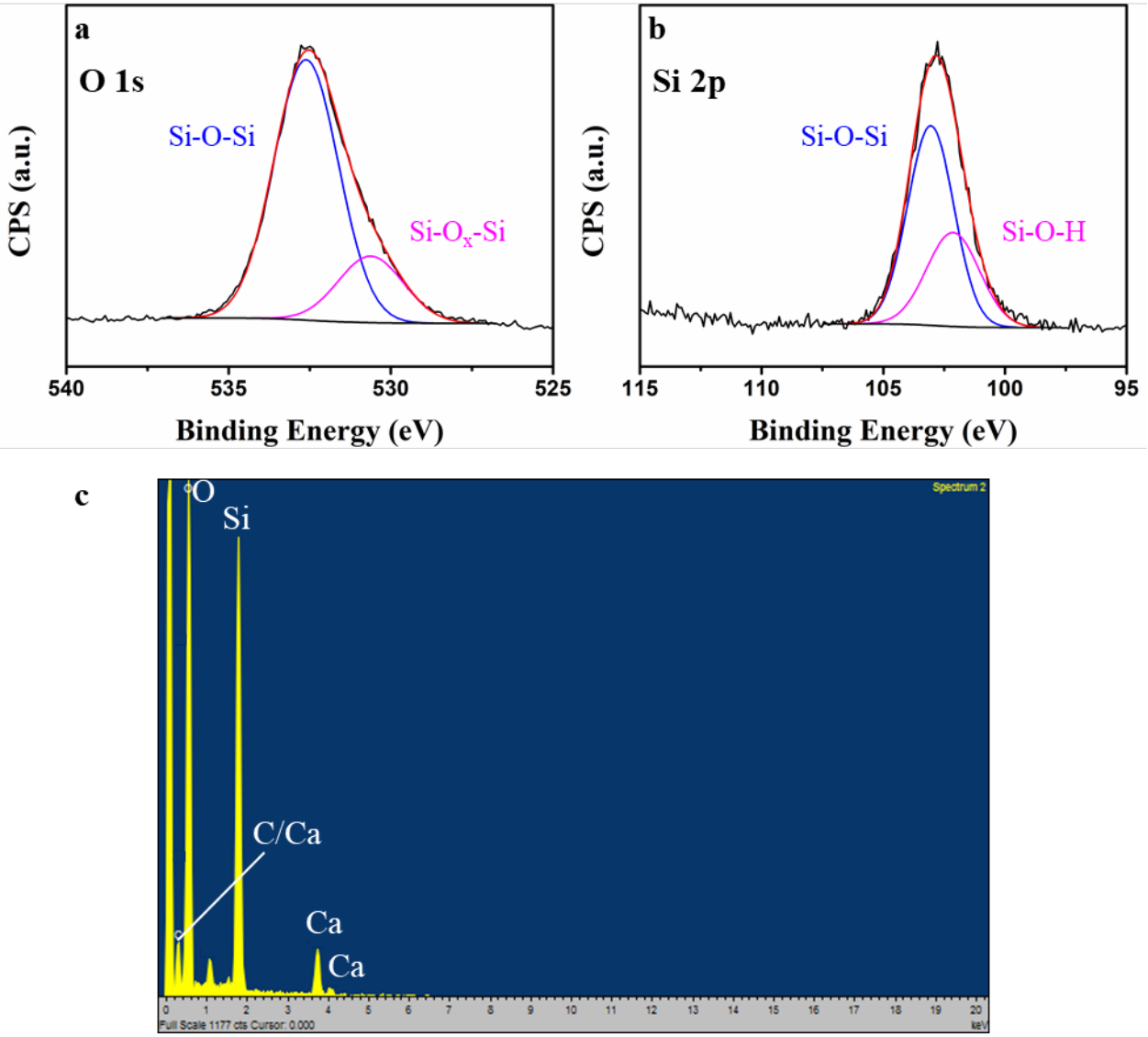

Fig. 10 XPS spectra of (a) O 1s and (b) Si 2p peaks of R1 (486 µL sodium silicate, 20 mg NaCas, and 8 mmol L^{-1} $CaCl_2$). Red curve is the cumulative fitting. (c) EDX data for R1

They key components of the modified-Stöber process involved in the formation of spherical silica particles are the SDA, such as CTAB and ammonium hydroxide. CTAB forms micelles in solution when the critical micelle concentration (cmc) is reached. The silica precursor is hydrolysed within the core of these micelles and subsequent condensation occurs with and around these micelles. The ammonium hydroxide acts as a catalyst for hydrolysis and also prevents agglomeration of the formed particles by stabilising the surface of the particles. This templated approach is driven by electrostatic and thermodynamic forces between the hydrolysed silicate species and the SDA (Alothman 2012). This micellar action of SDAs like CTAB is key to the formation of spherical silica particles. NaCas has similar properties to CTAB. As discussed, NaCas can form micelles in solution, but gives polydisperse spherical particles. However with the addition of calcium, the micelle structure of casein is stabilised, creating a more monodisperse structure (Smialowska et al. 2017). This is seen in our results. When calcium is added to our system, the monodispersity of the silica particles is greatly increased. In the absence of calcium, the particles exhibit a wide size variation with multiple peaks in the PSD. Addition of calcium to the hydrophobically associated casein clusters, reforms the native micelle structure. This reformation occurs via calcium interaction with the phosphate and carboxylate groups on the protein (Curley et al. 1998).

The above DOE analysed the influence NaCas, sodium silicate, and $CaCl_2$ had on particle size while keeping the pH constant. Isolating these factors made for an easier analysis. It is known that sodium silicate undergoes hydrolysis under acidic conditions. From the results of our experiments, it is clear that this occurs at pH 5.94 with subsequent condensation and morphological control provided by NaCas. However, to test whether this was true under different pH conditions, we conducted similar experiments at pH 4.94. **Fig. 11** shows SEM images of particles formed at pH 4.94. **Fig. 12** shows the corresponding DLS data for these experiments. The data show that

spherical particles were formed in each case. **Fig. 12a** shows that particles of diameter 264 nm with PDI of 0.223 were formed with 40 mg NaCas. Increasing the amount of NaCas to 80 mg decreases the particle size to 254 nm, while lowering the PDI to 0.168 (**Fig. 12b**). Further increasing the amount of NaCas to 120 mg decreases the particle size to 228 nm, with no significant change of the PDI (**Fig. 12c**). However, increasing the amount of NaCas to 160 mg increases the particle size to 275 nm, while also increasing the PDI to 0.212 (**Fig. 12d**). While this system also produces relatively monodisperse particles, increasing the amount of NaCas generally results in smaller particles. This is contrary to the system at pH 5.94, where **Eqn. 1** predicts an increase in particle size with increasing NaCas. This difference in particle size response under different pH might be explained by having increased electrostatic repulsion between forming particles at lower pH. However, further work is needed to understand this dependence.

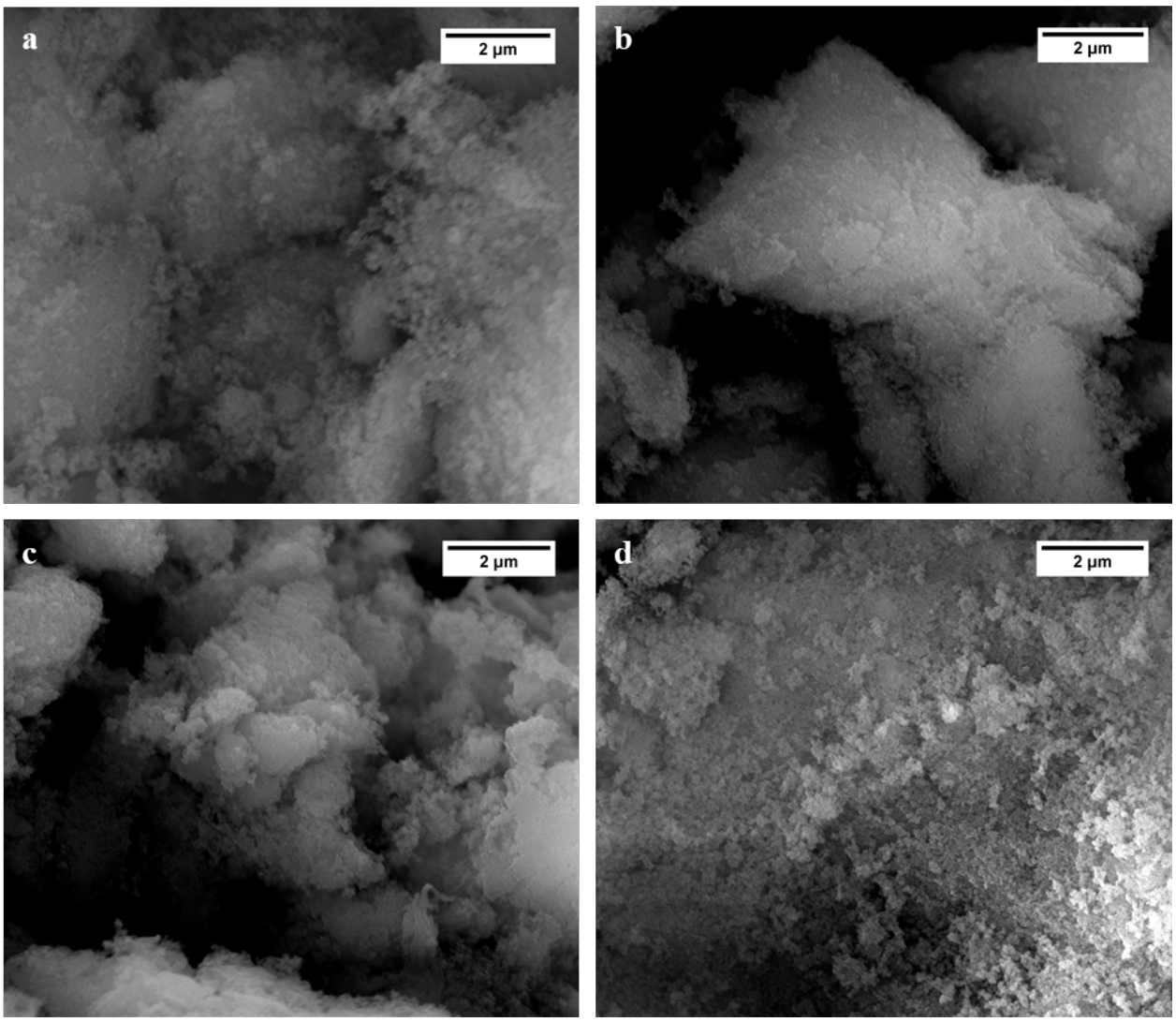

Fig. 11 SEM micrographs of silica prepared with (a) 40 mg NaCas (BC1), and (b) 80 mg NaCas (BC2), (c) 120 mg NaCas (BC3), and (d) 160 mg NaCas (BC4). Scale bars = 1 µm. All other reactants kept constant

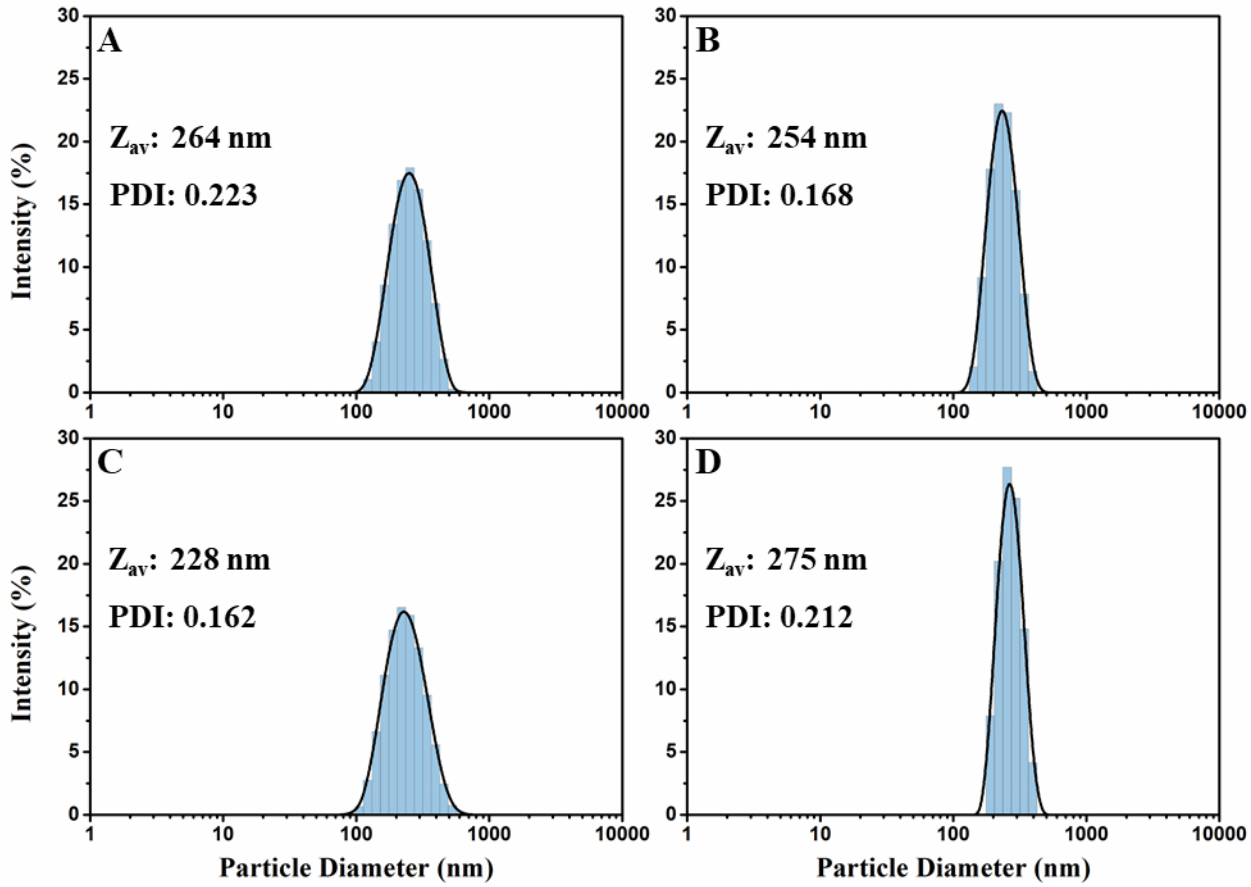

Fig. 12 PSDs from DLS measurements of silica prepared with (a) 40 mg NaCas (BC1), and (b) 80 mg NaCas (BC2), (c) 120 mg NaCas (BC3), and (d) 160 mg NaCas (BC4). All reactions used 729 µL sodium silicate and 8 mmol L^{-1} $CaCl_2$, in 50 mL acetate buffer (0.05 mol L^{-1}, pH 4.94)

We have shown that it is possible to synthesise spherical silica particles more sustainably than the Stöber processes. It is envisaged that such sustainable processes will ultimately succeed the Stöber processes, especially for larger-scale syntheses. However, the work detailed here is only a tentative step in that direction. Particle durability compared to other synthesis methods is an interesting aspect to focus on. Although it wasn't within the scope of our study, this could be a valuable focus of future work. Furthermore, there are infrastructural barriers around municipal and industrial water treatment and processing that must be addressed for water-based chemistries to be economically feasible at industrial scales. These issues are beyond the scope of our work but are

an ongoing focus of the UN Sustainable Development Goals, numerous state circular economy initiatives, and various governmental and non-governmental green chemistry initiatives. However, using biopolymers from waste streams of global scale industrial processes, such as caseinate from diary production wastes, means that one can obtain large amounts of the desired biopolymers from these processes. In the case of dairy products, these are subject to increasing global demand year-on-year, guaranteeing a steady supply of the necessary biopolymer. It is important to note, however, that industries like dairy production generate large greenhouse gas emissions, and future, regular life-cycle analyses should be part of any development of circular economies and green chemistries – within silica manufacture and without – to ensure that valorisation of waste streams does not lead to maintenance of damaging industries that would otherwise fail economically without such valorisation.

The use of biopolymers from valorised waste streams and the general reduction of organic reagents in industrial processes reduces the embedded costs associated with petrochemical production and refinement. This is not to say that there are no greenhouse gas emissions embedded in the production of biopolymers – of course there are. These will arise particularly from processes needed to isolate them from waste streams, and from the use of water-based chemistries, which currently requires far more energy to purify than organic solvents do. Part of the issue here is the lack of development of industrial water purification infrastructures, which could lead to greater efficiencies in this area. The highest priority problem to be solved for the planet right now is that of human driven climate change and that means first and foremost we must reduce greenhouse gas emissions. The work presented here shows that producing spherical and monodisperse silica particles is possible using biopolymer-based syntheses and water-based chemistries, and this is a small step towards achieving that.

Conclusion

We have successfully developed a sustainable synthesis for producing size-monodisperse spherical silica particles. Sodium caseinate was shown to act as a structure-directing agent to form spherical silica, and an effective replacement for petrochemically-derived surfactants such as CTAB. Using sodium caseinate, sodium silicate, and acetate buffer, spherical particles exhibiting polydispersity were formed in the size range 124 – 1588 nm. Incorporating calcium chloride into the synthesis stabilised the casein micelles to produce monodisperse spherical silica nanoparticles in the size range 172 – 340 nm. We optimised this process further through a statistical design of experiments that led to the development of a regression equation that we could use to predict particle size based on input concentrations. Our experimentally produced particles were in good agreement (> 90%) with these predicted sizes. Monodisperse particles were produced at pH 5.94 and pH 4.94. Our process uses sodium caseinate, sodium silicate, calcium chloride, and acetate buffer to produce silica nanoparticles in an environmentally friendly and sustainable way.

Declarations

Funding

This research was funded by AMBER through Science Foundation Ireland (Grant No.: 12/RC/2278) and Glantreo Ltd.

Conflicts of interest/Competing interests

On behalf of all authors, the corresponding author states that there is no conflict of interest.

Data availability

All data included in the manuscript is available.

Acknowledgements

We wish to thank Dr. John Hanrahan for useful discussions and Dr. Joe McGrath for running the BET analysis.

References

Alothman Z (2012) A Review: Fundamental Aspects of Silicate Mesoporous Materials. Materials (Basel) 5:2874–2902. https://doi.org/10.3390/ma5122874

Bao Y, Wang T, Kang Q, et al (2017) Micelle-template synthesis of hollow silica spheres for improving water vapor permeability of waterborne polyurethane membrane. Sci Rep 7:46638. https://doi.org/10.1038/srep46638

Belyakova LE, Antipova AS, Semenova MG, et al (2003) Effect of sucrose on molecular and interaction parameters of sodium caseinate in aqueous solution: relationship to protein gelation. Colloids Surfaces B Biointerfaces 31:31–46. https://doi.org/10.1016/S0927-7765(03)00041-9

Bhattacharjee S (2016) DLS and zeta potential – What they are and what they are not ? J Control Release 235:337–351. https://doi.org/10.1016/j.jconrel.2016.06.017

Bonnet C, Corredig M, Alexander M (2005) Stabilization of Caseinate-Covered Oil Droplets during Acidification with High Methoxyl Pectin. J Agric Food Chem 53:8600–8606. https://doi.org/10.1021/jf0511998

Capello C, Fischer U, Hungerbühler K (2007) What is a green solvent? A comprehensive framework for the environmental assessment of solvents. Green Chem 9:927–934. https://doi.org/10.1039/b617536h

Chen Y, Feng Y, Deveaux JG, et al (2019) Biomineralization Forming Process and Bio-inspired Nanomaterials for Biomedical Application: A Review. Minerals 9:68. https://doi.org/10.3390/min9020068

Chien S-C, Pérez-Sánchez G, Gomes JRB, et al (2017) Molecular Simulations of the Synthesis of Periodic Mesoporous Silica Phases at High Surfactant Concentrations. J Phys Chem C 121:4564–4575. https://doi.org/10.1021/acs.jpcc.6b09429

Coradin T, Coupé A, Livage J (2003) Interactions of bovine serum albumin and lysozyme with sodium silicate solutions. Colloids Surfaces B Biointerfaces 29:189–196. https://doi.org/10.1016/S0927-7765(02)00208-4

Coradin T, Durupthy O, Livage J (2002) Interactions of amino-containing peptides with sodium silicate and colloidal silica: A biomimetic approach of silicification. Langmuir 18:2331–2336

Curley DM, Kumosinski TF, Unruh JJ, Farrell HM (1998) Changes in the Secondary Structure of Bovine Casein by Fourier Transform Infrared Spectroscopy: Effects of Calcium and Temperature. J Dairy Sci 81:3154–3162. https://doi.org/10.3168/jds.S0022-0302(98)75881-3

Danaei M, Dehghankhold M, Ataei S, et al (2018) Impact of Particle Size and Polydispersity Index on the Clinical Applications of Lipidic Nanocarrier Systems. Pharmaceutics 10:57. https://doi.org/10.3390/pharmaceutics10020057

Demadis KD, Pachis K, Ketsetzi A, Stathoulopoulou A (2009) Bioinspired control of colloidal silica in vitro by dual polymeric assemblies of zwitterionic phosphomethylated chitosan and polycations or polyanions. Adv Colloid Interface Sci 151:33–48. https://doi.org/10.1016/j.cis.2009.07.005

Dickinson E, Semenova MG, Belyakova LE, et al (2001) Analysis of Light Scattering Data on the Calcium Ion Sensitivity of Caseinate Solution Thermodynamics: Relationship to Emulsion Flocculation. J Colloid Interface Sci 239:87–97. https://doi.org/10.1006/jcis.2001.7480

Gautier C, Abdoul-Aribi N, Roux C, et al (2008) Biomimetic dual templating of silica by polysaccharide/protein assemblies. Colloids Surfaces B Biointerfaces 65:140–145. https://doi.org/10.1016/j.colsurfb.2008.03.005

Huppertz T, Fox PF, Kelly AL (2018) The caseins: Structure, stability, and functionality, Second Edi. Elsevier Ltd.

Jackson E, Correa S, Betancor L (2020) In Situ Immobilization of Enzymes in Biomimetic Silica. pp 259–270

Ji J, Zhang J, Chen J, et al (2015) Preparation and stabilization of emulsions stabilized by mixed sodium caseinate and soy protein isolate. Food Hydrocoll 51:156–165. https://doi.org/10.1016/j.foodhyd.2015.05.013

Jia J, Zhou X, Caruso RA, Antonietti M (2004) Synthesis of Microporous Silica Templated by Gelatin. Chem Lett 33:202–203. https://doi.org/10.1246/cl.2004.202

Keane DA, Hanrahan JP, Copley MP, et al (2010) A modified Stöber process for the production of mesoporous Sub 2 micron silica microspheres; applications in HPLC. J Porous Mater 17:145–152. https://doi.org/10.1007/s10934-009-9274-7

Knepper TP, Berna JL (2003) Surfactants: Properties, production, and environmental Aspects. pp 1–49

Kotzsch A, Gröger P, Pawolski D, et al (2017) Silicanin-1 is a conserved diatom membrane protein involved in silica biomineralization. BMC Biol 15:9–11. https://doi.org/10.1186/s12915-017-0400-8

Lamastra FR, Mori S, Cherubini V, et al (2017) A new green methodology for surface modification of diatomite filler in elastomers. Mater Chem Phys 194:253–260. https://doi.org/10.1016/j.matchemphys.2017.03.050

Li S, Chen F, Lin F, et al (2018) Adsorption Performance of SiO2/CPAM Composites for Aqueous Ca(II). BioResources 13:. https://doi.org/10.15376/biores.13.2.3554-3570

Lifshitz IM, Slyozov VV (1961) The kinetics of precipitation from supersaturated solid solutions. J Phys Chem Solids 19:35–50. https://doi.org/10.1016/0022-3697(61)90054-3

Lopez P, Gautier C, Livage J, Coradin T (2006) Mimicking Biogenic Silica Nanostructures Formation. Curr Nanosci 1:73–83. https://doi.org/10.2174/1573413052953156

Manzano M, Vallet-Regí M (2020) Mesoporous Silica Nanoparticles for Drug Delivery. Adv Funct Mater 30:1902634. https://doi.org/10.1002/adfm.201902634

Mason S, Young S, Araga M, et al (2019) Stain control with two experimental dentin hypersensitivity toothpastes containing spherical silica: a randomised, early-phase development study. BDJ Open 5:8. https://doi.org/10.1038/s41405-019-0016-x

McMahon DJ, Oommen BS (2013) Casein Micelle Structure, Functions, and Interactions. In: Advanced Dairy Chemistry. Springer US, Boston, MA, pp 185–209

Mohammadpour Dounighi N, Eskandari R, Avadi M, et al (2012) Preparation and in vitro

characterization of chitosan nanoparticles containing Mesobuthus eupeus scorpion venom as an antigen delivery system. J Venom Anim Toxins Incl Trop Dis 18:44–52. https://doi.org/10.1590/S1678-91992012000100006

Nałęcz-Jawecki G, Grabińska-Sota E, Narkiewicz P (2003) The toxicity of cationic surfactants in four bioassays. Ecotoxicol Environ Saf 54:87–91. https://doi.org/10.1016/S0147-6513(02)00025-8

Patwardhan S V, Staniland SS (2019) Biomineralisation: how Nature makes nanomaterials. In: Green Nanomaterials: From bioinspired synthesis to sustainable manufacturing of inorganic nanomaterials. IOP Publishing

Post P, Wurlitzer L, Maus-Friedrichs W, Weber A (2018) Characterization and Applications of Nanoparticles Modified in-Flight with Silica or Silica-Organic Coatings. Nanomaterials 8:530. https://doi.org/10.3390/nano8070530

Rasheed T, Nabeel F, Raza A, et al (2019) Biomimetic nanostructures/cues as drug delivery systems: a review. Mater Today Chem 13:147–157. https://doi.org/10.1016/j.mtchem.2019.06.001

Sabu C, Rejo C, Kotta S, Pramod K (2018) Bioinspired and biomimetic systems for advanced drug and gene delivery. J Control Release 287:142–155. https://doi.org/10.1016/j.jconrel.2018.08.033

Scully SM, Orlygsson J (2019) Biological Production of Alcohols. In: Advanced Bioprocessing for Alternative Fuels, Biobased Chemicals, and Bioproducts. Elsevier, pp 83–108

Sheikhpour M, Barani L, Kasaeian A (2017) Biomimetics in drug delivery systems: A critical review. J Control Release 253:97–109. https://doi.org/10.1016/j.jconrel.2017.03.026

Sierra L, Guth JL (1999) Synthesis of mesoporous silica with tunable pore size from sodium silicate solutions and a polyethylene oxide surfactant. Microporous Mesoporous Mater 27:243–253. https://doi.org/10.1016/S1387-1811(98)00258-3

Sing KSW, Williams RT (2004) Physisorption Hysteresis Loops and the Characterization of Nanoporous Materials. Adsorpt Sci Technol 22:773–782. https://doi.org/10.1260/0263617053499032

Smialowska A, Merino LM-, Ingham B, Carr AJ (2017) Effect of calcium on the aggregation behaviour of caseinates. Colloids Surfaces A Physicochem Eng Asp. https://doi.org/10.1016/j.colsurfa.2017.02.074

Sobańska AW (2020) Emerging or Underestimated Silica-Based Stationary Phases in Liquid Chromatography. Crit Rev Anal Chem 1–25. https://doi.org/10.1080/10408347.2020.1760782

Thommes M (2010) Physical Adsorption Characterization of Nanoporous Materials. Chemie Ing Tech 82:1059–1073. https://doi.org/10.1002/cite.201000064

Trejo R, Harte F (2010) The effect of ethanol and heat on the functional hydrophobicity of casein micelles. J Dairy Sci 93:2338–2343. https://doi.org/10.3168/jds.2009-2918

van Dokkum HP, Hulskotte JHJ, Kramer KJM, Wilmot J (2004) Emission, Fate and Effects of Soluble Silicates (Waterglass) in the Aquatic Environment. Environ Sci Technol 38:515–521. https://doi.org/10.1021/es0264697

Wagner C (1961) Theorie der Alterung von Niederschlägen durch Umlösen (Ostwald-Reifung). Berichte der Bunsengesellschaft für Phys Chemie 65:581–591. https://doi.org/10.1002/BBPC.19610650704

Walcarius A (2018) Silica-based electrochemical sensors and biosensors: Recent trends. Curr Opin Electrochem 10:88–97. https://doi.org/10.1016/j.coelec.2018.03.017

Xi Y, Liu B, Jiang H, et al (2020) Sodium caseinate as a particulate emulsifier for making indefinitely recycled pH-responsive emulsions. Chem Sci 11:3797–3803. https://doi.org/10.1039/C9SC05050G

Yang G-Z, Wibowo D, Yun J-H, et al (2017) Biomimetic Silica Nanocapsules for Tunable Sustained Release and Cargo Protection. Langmuir 33:5777–5785. https://doi.org/10.1021/acs.langmuir.7b00590

Yang G, Liu Y, Jin S, Zhao C (2020) Development of Core-Shell Nanoparticle Drug Delivery Systems Based on Biomimetic Mineralization. ChemBioChem 21:2871–2879. https://doi.org/10.1002/cbic.202000105

Yerramilli M, Ghosh S (2017) Long-term stability of sodium caseinate-stabilized nanoemulsions. J Food Sci Technol 54:82–92. https://doi.org/10.1007/s13197-016-2438-y

Zheng H, Poon CS, Li W (2020) Mechanistic study on initial passivation and surface chemistry of steel bars in nano-silica cement pastes. Cem Concr Compos 112:103661. https://doi.org/10.1016/j.cemconcomp.2020.103661